

# Fractional quantum Hall edge polaritons

Lucas Winter\* and Oded Zilberberg  
*Fachbereich Physik, Universität Konstanz, DE-78457 Konstanz, Germany*  
(Dated: August 24, 2023)

It is commonly believed that light cannot couple to the collective excitations of the fractional quantum Hall effect (FQHE). This assumption relies on Kohn's theorem that states that electron-electron interactions decouple from homogeneous electromagnetic fields due to galilean invariance. Here, we demonstrate that the existence of an edge breaks Kohn's theorem, and enables coupling of cavity light to the plasmonic edge modes of the FQHE. We derive the coupling using the FQHE bulk-boundary correspondence and predict the formation of experimentally detectable plasmon polaritons. We find that a single cavity mode leaves the system's topological protection intact. Interestingly, however, a multimode cavity mediates plasmon backscattering, and effectively transforms the edges of the 2D FQHE into a 1D wire. Such cavity-mediated nonlocal backscattering bodes the breakdown of the topological protection in the regime of ultra-strong photon-plasmon coupling. Our analytical framework and photoelectric findings pave the way for investigating the topological order of the FQHE via optical spectroscopic probes and provide new opportunities to control FQHE edge excitations using light.

One of the most fascinating effects in condensed matter physics is the emergence of collective excitations arising from strong interactions between particles [1, 2]. A principal setting for the formation of such exotic quasiparticles is the fractional quantum Hall effect (FQHE) [3–8]. Here, electrons with charge  $e$  and mass  $m$  are confined to move in 2D in the presence of a perpendicular magnetic field  $B$ . The competition between their kinetic energy and the magnetic field suppresses the dispersion, and leads to cyclotron motion at frequency  $\omega_c = eB/m$ . As a result, a highly-degenerate Landau-level spectrum with gaps  $\hbar\omega_c$  manifests. In this setting, electron-electron interactions can dominate and open a many-body gap at specific fractional fillings of the Landau levels, where new quasiparticles emerge. These collective excitations are dubbed anyons and are predicted to obey fractional exchange statistics, i.e., they are neither bosonic nor fermionic [7, 9, 10], and can even be used for topological quantum computation [11, 12]. Relevant for this work, at so-called Laughlin fillings  $\nu = 1/(2p+1)$  with  $p \in \mathbb{N}$  [3, 13, 14], the resulting FQHE is well-described using composite fermions (CFs) that support anyonic bulk excitations with energy scales on the order of the Coulomb energy  $\sim e^2/(\epsilon l_B)$ , where  $\epsilon$  is the dielectric constant and  $l_B$  is the magnetic length [6].

Strong light-matter coupling in optical cavities can also lead to interesting collective excitations and effects [15–17]. For example, it allows for novel topological phases populated by light-matter hybrid particles known as polaritons [18, 19]. In relation to the quantum Hall effect, coupling to light was used both for probing and for modifying the topological order using cavities [20–27]. In the non-interacting limit, and using very high frequencies, transitions between Landau levels were studied, leading to the formation of Landau polaritons [28–31], and modification of the quantized electron transport of the integer quantum Hall effect (IQHE) [32–34]. In essence, cavity

vacuum fluctuations tend to expunge the quantized Hall transport in the IQHE [34–38]. Moving to the FQHE, its topological order can be probed indirectly by Landau polaritons [39, 40]. Furthermore, the induction of bulk anyonic excitations by locally inserting angular momentum with electric fields has been proposed [41]. However, in experiments, the FQHE shows significant resilience to such coupling [35]. This resilience stems from Kohn's theorem, which states that a homogeneous electromagnetic field only modifies the center of motion dynamics while leaving electron-electron correlations intact. For the same reason, the topological order seems to be protected from cavity vacuum fluctuation [35, 38].

In realistic scenarios, however, Hall systems are finite. Due to the so-called bulk-boundary correspondence, chiral electronic edge modes appear in the gaps between the Landau levels, which carry the IQHE current [42, 43]. Crucial to this work, a similar bulk-boundary correspondence manifests for the CFs, and carries the fractionally-quantized current of the FQHE [7]. At the edge, we then expect chiral collective bosonic excitations (plasmonic modes), which fill the gaps between the effective CF Landau levels [44, 45]. As the boundary breaks the translational invariance of the system, it also nulls the argument of Kohn's theorem, leading to a mechanism by which the FQHE can couple to light.

In this work, we derive a model for the coupling between cavity light and the FQHE. Our derivation harnesses the bulk-boundary correspondence, and implies strong coupling with the system's plasmonic edge modes. As a result, edge polaritons appear, which can be observed experimentally. From the point of view of the matter, the cavity introduces backscattering between the edge modes on the opposite sides of the system, which may impact the Hall conductance. Interestingly, a single-mode cavity is insufficient to disturb the quantized conductance. Nevertheless, a multimode cavity leads to the

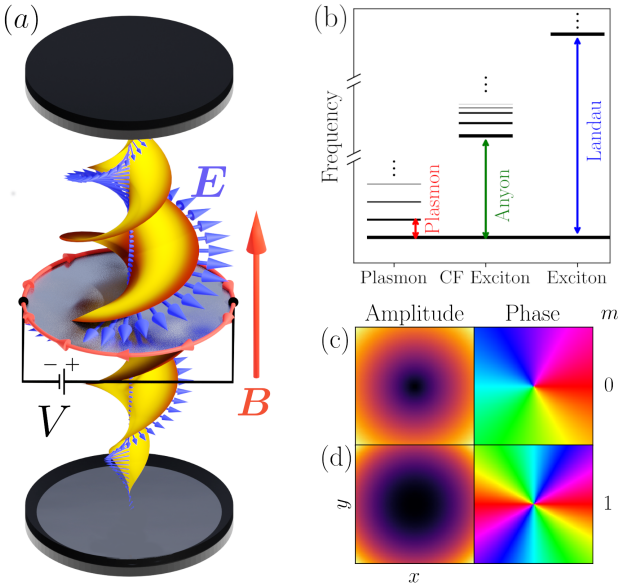


Figure 1. *System.* (a) A 2D Hall disc positioned inside an optical cavity, cf. Eq. (1). The Hall disc is subject to a perpendicular magnetic field  $\mathbf{B}$ , and is coupled to a circularly-polarized cavity mode  $\mathbf{E}$  (blue arrows) with a helical wavefront (orange surface). A voltage bias  $V$  can be applied across the edge of the Hall bar. (b) The hierarchy of energy scales of the Hall effect corresponding to potential excitation by the cavity. From small to large energies: FQHE edge plasmons (red), FQHE bulk excitations (green), and IQHE Landau-level spacing (blue). (c) and (d) Examples of the cavity mode's amplitude and phase in the plane of the Hall disc for different OAM quanta  $m$ , cf. Eq. (2).

proliferation of unstable polariton states, and a crossover to an insulator. In other words, the topological protection is lifted by the strong coupling to cavity light. We provide a variety of predictions, which are within experimental reach. At the same time, our methodology can be applied to a plethora of other topological systems in mesoscopics, as well as in quantum simulators.

We consider an optical cavity coupled to a spinless 2D electron gas (2DEG) in the FQHE regime [see Fig. 1(a)]

$$H_C = \frac{1}{2m_e}(\boldsymbol{\pi} - e\mathbf{A})^2 + V_{\text{int}} + V_{\text{conf}} + H_{\text{cav}}, \quad (1)$$

where  $\boldsymbol{\pi} = \mathbf{p} - eBx\hat{\mathbf{e}}_y$  is the canonical momentum of electrons moving in the plane with momentum  $\mathbf{p}$  in the presence of a perpendicular magnetic field  $B$ . The latter is written in Landau's gauge. The light-matter coupling involves the cavity vector potential  $\mathbf{A}$  using standard minimal coupling [6]. The terms  $V_{\text{int}}$  and  $V_{\text{conf}}$  are the electrons' Coulomb interaction and confinement potentials, respectively. The term  $H_{\text{cav}} = \sum_l \hbar\omega_{c,l} a_l^\dagger a_l$  describes a multimode cavity with mode frequencies  $\omega_{c,l}$  and quantized annihilation operators  $a_l$ . In Fig. 1(b), we summarize the hierarchy of energy scales of the FQHE, cf. Eq. (1) in the absence of the cavity, and the discussion

in the introduction.

For simplicity, we assume the system to be rotationally symmetric around the cavity axis. Hence, we can write the cavity electromagnetic field at the Hall disc plane using conserved angular momentum numbers,  $l$ ,

$$\mathbf{A} = \sum_{l>0} \mathbf{A}_l = \sum_{l>0} \epsilon^{l-1} a_l + \epsilon^*(z^*)^{l-1} a_l^\dagger, \quad (2)$$

where  $\epsilon = (1, i, 0)^T/\sqrt{2}$  is the circular polarization vector,  $a_l$  are photon (bosonic) annihilation operators, and  $z = (x + iy)/R$  encodes the position of electrons in the 2DEG using a complex coordinate, where  $R$  denotes the radius of the disc. Each cavity mode carries in total  $l$  quanta of angular momentum, consisting of one *quantum spin angular momentum* and  $m = l - 1$  quanta of *orbital angular momentum* (OAM) [46, 47], see Figs. 1(c) and (d). Note that the coupling of any 3D cavity field to a 2DEG can be written as in Eq. (2) by applying a suitable gauge transform and quantization in angular momentum modes [48].

In the following, we treat the coupling to the cavity perturbatively. As we are interested in coupling to low-energy excitations, we truncate matrix elements that couple to high energies, cf. Fig. 1(b). Our model (1), however, is written in the Coulomb gauge, i.e., the perturbative treatment is not compatible with such level truncation [49, 50]. Hence, we switch to the dipole gauge using the unitary transformation  $H_D = U H_C U^\dagger$  with  $U = \exp(-ie \sum_{l>0} \mathbf{A}_l \cdot \mathbf{r}/(l\hbar))$  [51]. During the transformation, we omit single-particle terms that are negligible in the strong-coupling limit [48], and obtain

$$H_D = \frac{\pi^2}{2m_e} + V_{\text{int}} + V_{\text{conf}} + \sum_{l>0} \frac{e}{l} \mathbf{E}_l \cdot \mathbf{r} + H_{\text{cav}}, \quad (3)$$

where  $\mathbf{E} = \sum_{l>0} \mathbf{E}_l$  is the electric field,  $\mathbf{E}_l \cdot \mathbf{r} = i A_{l,\omega_{c,l}} (p_l a_l - p_l^* a_l^\dagger)$ , and  $p_l = \sum_j z_j^l$  is a symmetric polynomial in the electron coordinates  $\{z_j\}$ .

When the FQHE system absorbs a photon  $a_l^\dagger$  [see Fig. 2(a)], angular momentum conservation dictates a transition to an excited state,  $|\Psi_l\rangle$ , with  $l$  additional quanta of angular momentum than the Laughlin ground state,  $|\Psi_0\rangle$ . This is represented as  $|\Psi_l\rangle = p_l |\Psi_0\rangle$  [13, 52, 53], where multiplying by the symmetric polynomial  $p_l = \sum_j z_j^l$  creates a superposition of states with an electron's angular momentum that is increased by  $l$  units through phase multiplication  $z^l \propto e^{i\varphi l}$ . As a result, the matrix elements of the light-matter coupling in the basis of  $|\Psi_l\rangle$  are

$$\langle \Psi_{l_1} | \mathbf{E}_l \cdot \mathbf{r} | \Psi_{l_2} \rangle = i E_l \left( \langle \Psi_{l_1} | p_l | \Psi_0 \rangle a_l - \langle \Psi_{l_1} | p_l | \Psi_0 \rangle^* a_l^\dagger \right), \quad (4)$$

with  $E_l = A_{l,\omega_{c,l}}$ . Note that we used the fact that  $|\Psi_l\rangle$  are orthogonal in the thermodynamic limit  $N \rightarrow \infty$  [54,

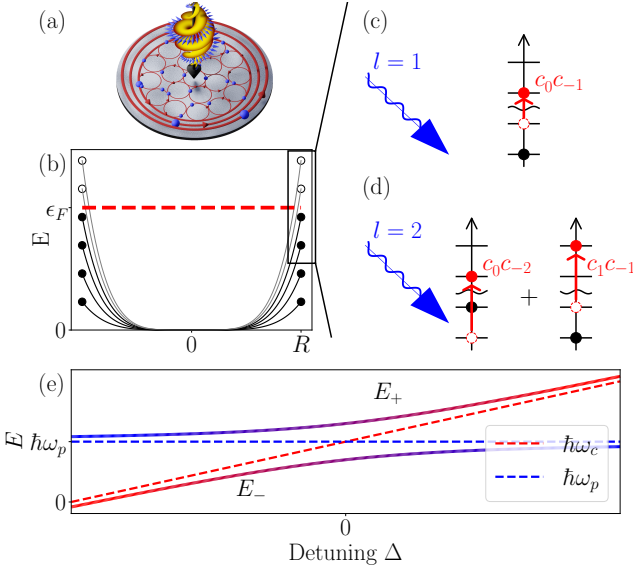


Figure 2. *Light-matter coupling to the FQHE and formation of edge plasmon-polaritons.* (a) A delocalized photonic mode interacts with the electrons of a FQHE disc. Red lines mark electron trajectories in the bulk and at the edge. (b) Electron energy levels for different angular momentum as a function of the distance  $r$  from the center. At the edge, the angular momentum degeneracy is lifted; black dots mark occupied angular momentum states below the Fermi energy  $\epsilon_F$  (red dashed line). (c) and (d) The interaction between light and matter induces a superposition of electrons with increased angular momentum [cf. Eq. (4)], forming a superposition of excitons on the edge. This interaction results in the formation of edge plasmons [56]. Black (red) dots mark filled electron levels above (below) the Fermi energy  $\epsilon_F$  [wiggly line]. Empty circles indicate unoccupied electron levels. (e) FQHE edge excitations spectrum in a single-mode cavity field shows plasmon-polariton anticrossing with cavity detuning [cf. Eq. (5)]. Dashed lines indicate the spectrum without light-matter interaction.

55]. Furthermore, the light-induced transitions are only “swirling” the FQHE droplet, i.e., they do not suffice to excite an excitation in the bulk.

Crucial to this work, the system’s bulk-edge correspondence states that each  $|\Psi_l\rangle$  represents a plasmonic surface wave at the edge. Specifically, at the boundary, we have a chiral Luttinger liquid (LL) edge, dubbed  $\chi_{\text{LL}}$  theory, that consists of the energy levels of the edge plasmons  $\hbar\omega_{pl}$  [44], see Fig. 2(b). To describe the coupling of the light to the edge, we can switch from the Hilbert space of bulk electrons to the Hilbert space of edge plasmons by exchanging  $p_l \leftrightarrow \sqrt{\nu l} L/(2\pi) b_l$  and  $p_l^* \leftrightarrow \sqrt{\nu l} L/(2\pi) b_l^\dagger$ , where  $\nu$  is the filling factor  $\nu = n_{2D}h/(eB)$  corresponding to electron density  $n_{2D}$ ,  $L$  is the edge circumference, and  $b_l$  are bosonic operators annihilating plasmonic surface waves [48, 54, 55]. In this step, the superposition of bulk electrons with added angular momentum  $l$ ,  $p_l = \sum_j z_j^l$  becomes a superposition of edge particle-hole

pairs  $b_q = i\sqrt{2\pi/(Lq)} \sum_{k \neq 0} c_{q+k}^\dagger c_k$ , where  $c_k$  annihilates an electron on the edge with linear momentum  $k$ , see Figs. 2(c) and (d) [56]. The resulting cavity-plasmon Hamiltonian at the edge reads

$$H_L = \sum_{l>0} \left[ \hbar\omega_{pl} b_l^\dagger b_l + \hbar\omega_{c,l} a_l^\dagger a_l + i\hbar g_l (b_l^\dagger a_l - b_l a_l^\dagger) \right], \quad (5)$$

where  $\omega_p = 2\pi v/L$  denotes the frequency of the lowest edge plasmon mode with  $v$  the edge drift velocity. The light-matter coupling reads  $g_l = eE_l L \sqrt{\nu} / \sqrt{4\pi^2 l \hbar^2} = eE_l \sqrt{\nu L} / \sqrt{2\pi k \hbar^2} \propto 1/\sqrt{k}$ , where  $k = 2\pi l/L$  is the plasmon’s wavevector. This implies that an absorbed photon, with angular momentum  $l$ , creates an edge plasmon with linear momentum  $k = 2\pi l/L$ , see Figs. 2(c) and (d). Crucially, the total angular momentum is thus conserved, as the Hall system can absorb both SAM and OAM. Furthermore, in the case of a cavity field with opposite chirality to that of the edge mode, we need to exchange  $a_l \leftrightarrow a_l^\dagger$  in Eq. (5), indicating that an absorbed photon destroys a plasmon. Note also that we can derive the photon-plasmon coupling through a cavity-induced anomalous current [57].

Strong light-matter coupling typically leads to the formation of polaritons [16]. For simplicity, we first consider a single-mode cavity with angular momentum  $l$ . Due to conservation of angular momentum, the cavity will couple solely to a single plasmon mode with momentum  $k = 2\pi l/L$ . We can diagonalize the Hamiltonian (5) via a Bogoliubov transform and obtain the polariton eigenenergies  $2E_{\pm} = \hbar\omega_{pl} + \hbar\omega_c \pm \sqrt{\Delta^2 + 4\hbar^2 g_l^2}$ , where  $\Delta = \hbar(\omega_c - \omega_{pl})$ . The resulting spectrum reveals the typical anti-crossing, see Fig. 2(d). Importantly, the anticrossing can be measured using spectroscopy experiments: using common experimental values [58–60], the plasmon velocity  $v$  for filling factor  $\nu = 1/3$  ranges in the interval:  $2 \cdot 10^4 - 4 \cdot 10^4$  m/s. Considering an edge length of  $L = 100\mu\text{m}$ , this results in a plasmon frequency,  $\omega_p = 2\pi v/L$ , of around 1 GHz, which is notably lower than the cyclotron frequency.

We next assess how coupling to the cavity mode affects conductivity, as measured at opposing points on the Hall disc. At opposite edges, we effectively have left-moving ( $q < 0$ ) and right-moving plasmonic excitations ( $q > 0$ ), see Fig. 3(a). Inverting the  $y$ -axis ( $\mathcal{T} : y \rightarrow -y$ ) morphs the left-moving edge into the right-moving edge. Thus, applying  $\mathcal{T}$  to the light-matter coupling Hamiltonian (5),  $\mathcal{T}H_{\text{int}}$ , yields the coupling term for the left-moving edge. Additionally, applying the inversion to the plasmon wavefunction coordinates leads to complex conjugation  $\mathcal{T}z = z^*$ , so  $\mathcal{T}b_q = b_{-q}^\dagger$ . Hence, together, the Hamiltonian containing both edges reads

$$H_{2E} = \sum_{q \neq 0} \left[ \hbar v |q| b_q^\dagger b_q + \hbar\omega_{c,l} a_{l,q}^\dagger a_{l,q} + i\hbar g_q (b_q^\dagger a_q - b_{-q}^\dagger a_{-q}^\dagger) \right], \quad (6)$$

where we use the convention  $a_{-q} = -a_q^\dagger$ . To ascertain

the effective cavity-mediated coupling between the left- and right-moving edge states, we apply a Schrieffer-Wolff transformation on  $H_{2E}$  and obtain

$$H_{\text{eff}} = \sum_{q \neq 0} \hbar|q| \left[ \left( v + V_1(q) \right) b_q^\dagger b_q + V_2(q) (b_q^\dagger b_{-q}^\dagger + b_q b_{-q}) \right]. \quad (7)$$

Here,  $V_1(q) = -g^2/(|q|(\omega_c - qv))$  and  $V_2(q) = -g^2\omega_c/(|q|(\omega_c^2 - v^2q^2))$  [48]. Importantly, we obtain the familiar Luttinger Hamiltonian for a 1D wire when the cavity is included [61]. Specifically, the cavity introduces plasmon backscattering proportional to  $V_2$ , see Fig. 3(a).

Using our effective (matter-only) model, we can compute the conductivity through the opposite edges of the device, see Fig. 1(a). To this end, we diagonalize the effective model (7) using a Bogoliubov transformation  $b_q^\dagger = \cosh(\varphi_q)\beta_q^\dagger - \sinh(\varphi_q)\beta_{-q}$ , where  $\tanh(2\varphi_q) = V_2/(v + V_1)$ , and  $b_q$  transforms accordingly [61]. In diagonal form, the model reads  $H_{\text{eff}} = \sum_{q \neq 0} \hbar v_q |q| \beta_q^\dagger \beta_q$ , with the sound velocity  $v_q = \sqrt{(v + V_1)^2 - V_2^2}$ . The current operator is defined by  $j_q = (i/q)\partial_t n_q$ , with  $n_q$  the electron density. In our case, the current operator linearized around small wavevectors reads  $j_q = \sqrt{\nu} \sqrt{L|q|/(2\pi)} v \operatorname{sgn}(q)(\beta_q - \beta_{-q})$  [56]. Using Kubo's formula for small wavevectors, the conductivity can be derived from the current operator and reads [62]

$$\sigma = \frac{e^2}{\hbar L} \int_{-\infty}^0 dx' \sum_{q \neq 0} e^{iq(x-x')} G_j(q, \omega), \quad (8)$$

where  $G_j(q, \omega) = i \int_0^\infty dt \langle [j_q(t), n_{-q}(0)] \rangle e^{i(\omega+in)t}$  is the retarded current-density correlation function, and the latter is obtained from the relation  $\beta_q^\dagger = e^{iv_q|q|t} \beta(0)$ .

Recall that a single-mode cavity with photon angular momentum  $l$  couples only to one plasmon mode with wavevector  $Q_c = 2\pi l/L$  as  $g_q = g \cdot \delta_{Q_c, q}$ . In this case, the sum in Eq. (8) can be written as

$$\begin{aligned} \sigma &= \frac{e^2 \nu}{h} + \frac{e^2}{\hbar L} \int_{-\infty}^0 dx' \sum_{q=\pm Q_c} e^{iq(x-x')} (\tilde{G}_j - G_j) \\ &= \frac{e^2 \nu}{h} \left( 1 + v \frac{\Delta t_q}{L} \sin(q_l x) \right), \end{aligned} \quad (9)$$

where  $\tilde{G}_j$  is the current-density correlation function in presence of the cavity and  $G_j$  is the one without it, and  $\Delta t_q = L/v_q - L/v_{-q}$  is the time-of-flight difference between excitations propagating on the two edges. For  $x = L$ , we obtain  $\sigma = e^2 \nu / h$ , implying that the conductivity remains unchanged. In other words, we find that a single cavity mode is insufficient to make a significant impact on the conductivity, which is consistent with recent experimental results [35]. At the same time, for  $x < L$ , the conductivity undergoes periodic modulation, a result of the chiral cavity field enhancing the group velocity on one edge while diminishing it on the other.

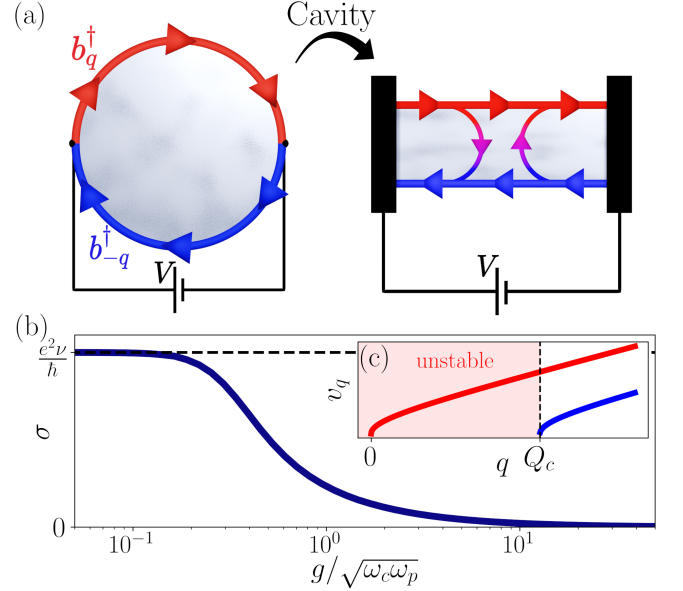


Figure 3. *Cavity mediated breakdown of topological protection* (a) The plasmons around the disc can be decomposed into right-moving (red) and left-moving (blue) modes. Cavity-mediated interactions couple the right- and left-movers and transform the system into an effective 1D wire. (b) The Hall conductivity, depicted as a function of photon-plasmon coupling strength for a drift velocity of  $v_p = 10^4$  m/s, a cyclotron frequency of  $\omega_{\text{cyc}} = 200$  GHz, and an edge length of  $L = 2\pi 10^{-5}$  m. (c) Backscattering splits the plasmon dispersion into two branches. The lower branch is pushed to zero frequency and becomes unstable below the wavevector  $Q_c = \frac{2g}{\omega_c v}$ .

We turn now to consider a multimode cavity with photon angular momenta  $l = 1, \dots, \infty$ . This can be achieved by increasing the uncertainty of the angular momentum  $\Delta L$ , e.g., by reducing the photon azimuthal angle  $\Delta\phi$ , as  $\Delta L \cdot \Delta\phi \geq \hbar/2$  due to the uncertainty relation. Experimentally, this can be accomplished by using a "pizza-slice aperture" [63]. For a long edge length  $L$  with plasmon momentum spacing  $\Delta q = 2\pi/L \ll 1$ , we can assume a continuum of modes. This allows us to replace the sum over  $q$  in Eq. (8) with an integral, and obtain

$$\sigma = \frac{e^2 \nu}{h} \sum_{s=\pm} \sum_j \lim_{q \rightarrow q_{s,j}} \left( (q - q_{s,j}) \frac{\omega + sv_{sq}|q|}{\omega^2 - v_{sq}^2 q^2} e^{iq(x-x_s)} \right). \quad (10)$$

Here,  $q_{j,s}$  represents a root of the polynomial  $\omega^2 - v_{sq}^2 q^2 = 0$ . The roots are found by computing the eigenvalues of the companion matrix of the polynomial [48].

In Fig. 3(b), we plot the resulting conductivity as a function of coupling strength. We observe a significant reduction in conductivity in the limit of ultrastrong photon-plasmon coupling where  $g > \sqrt{\omega_c \omega_p}$ . The conductivity decreases as more of the plasmon modes become gapped. In the continuum limit  $L \rightarrow \infty$ , we can express the plasmon sound velocity as  $v_{\pm q} = \sqrt{(vq \mp 2g^2/\omega_c)vq}$ .

The plasmon dispersion splits into two branches, see Fig. 3(c). The lower branch shifts to zero frequency and becomes unstable for plasmons with wavevector  $q$  smaller than  $q \leq Q_c = 2g^2/(\omega_c v)$ . As the strength of the light-matter coupling increases, more plasmon modes become unstable, inducing a crossover from a Chiral Luttinger liquid to a charge density wave insulator. The critical wavevector  $Q_c$  implies that the light-matter coupling threshold should scale as  $g_{\text{thresh}}/\omega_c \propto \sqrt{\omega_p/\omega_c}$ , as a function of cavity  $\omega_c$  and plasmon frequency  $\omega_p$ . Our theory could elucidate the light-induced transition from metal to charge density wave (CDW) in 1T-TaS<sub>2</sub> [64].

We derive a comprehensive analytical model describing the coupling of cavity light to the FQHE at Laughlin fractions. Three main implications of our result involve (i) the cavity modes can form polaritons with the plasmonic edges of the FQHE, (ii) a single-cavity mode is insufficient for impacting the quantized Hall conductance of the FQHE, and (iii) a multimode cavity can induce a crossover into an insulator, and remove the topological protection of the quantized Hall conductance. The latter is a result of light-induced backscattering between opposite edges of the Hall system. Our model provides a versatile platform for studying light-matter interaction in the FQHE, which can be readily extended to other filling fractions  $\nu \neq 1/(2p+1)$ , with multiple edge modes. We anticipate similar coupling between light and topological boundary modes in other systems that exhibit the chiral anomaly. Taking into account realistic experimental values, our predictions are within reach of experimental observation, and motivate spectroscopic methods for probing the topological order of the FQHE, as well as assist in resolving long-standing controversies concerning the system's edge structure. Interestingly, the decay of the edge plasmons into photons opens up the potential of controlling the orbital angular momentum of light. Beyond mesoscopics, our model can be applied cold atomic systems, as well as other quantum simulators.

We thank S. Simon, P. Rabl, C. Ciuti, and I. Carusotto for fruitful discussions. The authors acknowledge financial support from the Deutsche Forschungsgemeinschaft (DFG) - project number 449653034 and SFB1432.

---

\* lucas.winter@uni-konstanz.de

[1] I. V. Lerner, B. L. Althsuler, V. I. Falko, and T. Giamarchi, *Strongly Correlated Fermions and Bosons in Low-Dimensional Disordered Systems*, Vol. 72 (Springer Science & Business Media, 2002).

[2] E. Dagotto, Complexity in strongly correlated electronic systems, *Science* **309**, 257 (2005).

[3] D. C. Tsui, H. L. Stormer, and A. C. Gossard, Two-Dimensional Magnetotransport in the Extreme Quantum Limit, *Physical Review Letters* **48**, 1559 (1982).

[4] J. Fröhlich and U. M. Studer, Gauge invariance and current algebra in nonrelativistic many-body theory, *Reviews of modern physics* **65**, 733 (1993).

[5] H. L. Stormer, D. C. Tsui, and A. C. Gossard, The fractional quantum hall effect, *Reviews of Modern Physics* **71**, S298 (1999).

[6] J. K. Jain, *Composite Fermions* (Cambridge University Press, 2007).

[7] A. Stern, Anyons and the quantum hall effect—a pedagogical review, *Annals of Physics* **323**, 204 (2008).

[8] J. Fröhlich, Gauge invariance and anomalies in condensed matter physics, *Journal of Mathematical Physics* **64** (2023).

[9] G. Campagnano, O. Zilberberg, I. V. Gornyi, D. E. Feldman, A. C. Potter, and Y. Gefen, Hanbury brown-twiss interference of anyons, *Physical review letters* **109**, 106802 (2012).

[10] G. Campagnano, O. Zilberberg, I. V. Gornyi, and Y. Gefen, Hanbury Brown and Twiss correlations in quantum Hall systems, *Physical Review B* **88**, 235415 (2013).

[11] C. Nayak, S. H. Simon, A. Stern, M. Freedman, and S. D. Sarma, Non-abelian anyons and topological quantum computation, *Reviews of Modern Physics* **80**, 1083 (2008).

[12] O. Zilberberg, B. Braunecker, and D. Loss, Controlled-not gate for multiparticle qubits and topological quantum computation based on parity measurements, *Physical Review A* **77**, 012327 (2008).

[13] R. B. Laughlin, Anomalous Quantum Hall Effect: An Incompressible Quantum Fluid with Fractionally Charged Excitations, *Physical Review Letters* **50**, 1395 (1983).

[14] H. L. Stormer, Nobel Lecture: The fractional quantum Hall effect, *Reviews of Modern Physics* **71**, 875 (1999).

[15] M. Fleischhauer, A. Imamoglu, and J. P. Marangos, Electromagnetically induced transparency: Optics in coherent media, *Reviews of modern physics* **77**, 633 (2005).

[16] I. Carusotto and C. Ciuti, Quantum fluids of light, *Reviews of Modern Physics* **85**, 299 (2013).

[17] J. Bloch, I. Carusotto, and M. Wouters, Non-equilibrium bose-einstein condensation in photonic systems, *Nature Reviews Physics* **4**, 470 (2022).

[18] T. Ozawa, H. M. Price, A. Amo, N. Goldman, M. Hafezi, L. Lu, M. C. Rechtsman, D. Schuster, J. Simon, O. Zilberberg, *et al.*, Topological photonics, *Reviews of Modern Physics* **91**, 015006 (2019).

[19] D. D. Solnyshkov, G. Malpuech, P. St-Jean, S. Ravets, J. Bloch, and A. Amo, Microcavity polaritons for topological photonics, *Optical Materials Express* **11**, 1119 (2021).

[20] F. Schlawin, D. M. Kennes, and M. A. Sentef, Cavity quantum materials, *Applied Physics Reviews* **9**, 011312 (2022).

[21] A. Frisk Kockum, A. Miranowicz, S. De Liberato, S. Savasta, and F. Nori, Ultrastrong coupling between light and matter, *Nature Reviews Physics* **1**, 19 (2019).

[22] P. Forn-Díaz, L. Lamata, E. Rico, J. Kono, and E. Solano, Ultrastrong coupling regimes of light-matter interaction, *Reviews of Modern Physics* **91**, 025005 (2019).

[23] T. Jaako, Z.-L. Xiang, J. J. Garcia-Ripoll, and P. Rabl, Ultrastrong-coupling phenomena beyond the Dicke model, *Physical Review A* **94**, 033850 (2016).

[24] M. Ruggenthaler, N. Tancogne-Dejean, J. Flick, H. Apfel, and A. Rubio, From a quantum-electrodynamical

light-matter description to novel spectroscopies, *Nature Reviews Chemistry* **2**, 1 (2018).

[25] F. J. Garcia-Vidal, C. Ciuti, and T. W. Ebbesen, Manipulating matter by strong coupling to vacuum fields, *Science* **373**, eabd0336 (2021).

[26] M. A. Sentef, M. Ruggenthaler, and A. Rubio, Cavity quantum-electrodynamical polaritonically enhanced electron-phonon coupling and its influence on superconductivity, *Science Advances* **4**, eaau6969 (2018).

[27] P. Kirton, M. M. Roses, J. Keeling, and E. G. Dalla Torre, Introduction to the Dicke Model: From Equilibrium to Nonequilibrium, and Vice Versa, *Advanced Quantum Technologies* **2**, 1800043 (2019).

[28] D. Hagenmüller, S. De Liberato, and C. Ciuti, Ultrastrong coupling between a cavity resonator and the cyclotron transition of a two-dimensional electron gas in the case of an integer filling factor, *Physical Review B* **81**, 235303 (2010).

[29] G. Scalari, C. Maissen, D. Turčinková, D. Hagenmüller, S. De Liberato, C. Ciuti, C. Reichl, D. Schuh, W. Wegscheider, M. Beck, and J. Faist, Ultrastrong Coupling of the Cyclotron Transition of a 2D Electron Gas to a THz Metamaterial, *Science* **335**, 1323 (2012).

[30] J. Keller, G. Scalari, F. Appugliese, S. Rajabali, M. Beck, J. Haase, C. A. Lehner, W. Wegscheider, M. Failla, M. Myronov, D. R. Leadley, J. Lloyd-Hughes, P. Nataf, and J. Faist, Landau polaritons in highly nonparabolic two-dimensional gases in the ultrastrong coupling regime, *Physical Review B* **101**, 075301 (2020).

[31] X. Li, M. Bamba, Q. Zhang, S. Fallahi, G. C. Gardner, W. Gao, M. Lou, K. Yoshioka, M. J. Manfra, and J. Kono, Vacuum Bloch-Siegert shift in Landau polaritons with ultra-high cooperativity, *Nature Photonics* **12**, 324 (2018).

[32] N. Bartolo and C. Ciuti, Vacuum-dressed cavity magnetotransport of a two-dimensional electron gas, *Physical Review B* **98**, 205301 (2018).

[33] G. L. Paravicini-Bagliani, F. Appugliese, E. Richter, F. Valmorra, J. Keller, M. Beck, N. Bartolo, C. Rössler, T. Ihn, K. Ensslin, C. Ciuti, G. Scalari, and J. Faist, Magneto-transport controlled by Landau polariton states, *Nature Physics* **15**, 186 (2019).

[34] C. Ciuti, Cavity-mediated electron hopping in disordered quantum Hall systems, *Physical Review B* **104**, 155307 (2021).

[35] F. Appugliese, J. Enkner, G. L. Paravicini-Bagliani, M. Beck, C. Reichl, W. Wegscheider, G. Scalari, C. Ciuti, and J. Faist, Breakdown of topological protection by cavity vacuum fields in the integer quantum Hall effect, *Science* **375**, 1030 (2022).

[36] V. Rokaj, M. Penz, M. A. Sentef, M. Ruggenthaler, and A. Rubio, Quantum Electrodynamical Bloch Theory with Homogeneous Magnetic Fields, *Physical Review Letters* **123**, 047202 (2019).

[37] V. Rokaj, M. Penz, M. A. Sentef, M. Ruggenthaler, and A. Rubio, Polaritonic Hofstadter butterfly and cavity control of the quantized Hall conductance, *Physical Review B* **105**, 205424 (2022).

[38] V. Rokaj, J. Wang, J. Sous, M. Penz, M. Ruggenthaler, and A. Rubio, On the Topological Protection of the Quantum Hall Effect in a Cavity (2023), arxiv:2305.10558 [cond-mat].

[39] P. Knüppel, S. Ravets, M. Kroner, S. Fält, W. Wegscheider, and A. Imamoglu, Nonlinear optics in the fractional quantum Hall regime, *Nature* **572**, 91 (2019).

[40] P. Knüppel, *Two-Dimensional Polaron-Polaritons: Interactions and Transport*, Ph.D. thesis, ETH Zurich (2021).

[41] T. Graß, M. Gullans, P. Bienias, G. Zhu, A. Ghazaryan, P. Ghaemi, and M. Hafezi, Optical control over bulk excitations in fractional quantum Hall systems, *Physical Review B* **98**, 155124 (2018).

[42] R. B. Laughlin, Quantized Hall conductivity in two dimensions, *Physical Review B* **23**, 5632 (1981).

[43] B. I. Halperin, Quantized Hall conductance, current-carrying edge states, and the existence of extended states in a two-dimensional disordered potential, *Physical Review B* **25**, 2185 (1982).

[44] X. G. Wen, Chiral Luttinger liquid and the edge excitations in the fractional quantum Hall states, *Physical Review B* **41**, 12838 (1990).

[45] X.-G. Wen, THEORY OF THE EDGE STATES IN FRACTIONAL QUANTUM HALL EFFECTS — *International Journal of Modern Physics B* (1992).

[46] M. Padgett, J. Courtial, and L. Allen, Light's Orbital Angular Momentum, *Physics Today* **57**, 35 (2004).

[47] K. A. Forbes and D. L. Andrews, Orbital angular momentum of twisted light: chirality and optical activity, *Journal of Physics: Photonics* **3**, 022007 (2021).

[48] See supplemental material for more details.

[49] D. De Bernardis, P. Pilar, T. Jaako, S. De Liberato, and P. Rabl, Breakdown of gauge invariance in ultrastrong-coupling cavity QED, *Physical Review A* **98**, 053819 (2018).

[50] O. Di Stefano, A. Settineri, V. Macrì, L. Garziano, R. Stassi, S. Savasta, and F. Nori, Resolution of gauge ambiguities in ultrastrong-coupling cavity quantum electrodynamics, *Nature Physics* **15**, 803 (2019).

[51] J. D. Jackson, From Lorenz to Coulomb and other explicit gauge transformations, *American Journal of Physics* **70**, 917 (2002).

[52] F. Duncan and M. Haldane, The Hierarchy of Fractional States and Numerical Studies, in *The Quantum Hall Effect*, Graduate Texts in Contemporary Physics, edited by R. E. Prange and S. M. Girvin (Springer, New York, NY, 1990) pp. 303–352.

[53] S. H. Simon, Wavefunctionology: The Special Structure of Certain Fractional Quantum Hall Wavefunctions, in *Fractional Quantum Hall Effects* (WORLD SCIENTIFIC, 2020) pp. 377–434.

[54] J. Dubail, N. Read, and E. H. Rezayi, Edge-state inner products and real-space entanglement spectrum of trial quantum Hall states, *Physical Review B* **86**, 245310 (2012).

[55] R. Fern, R. Bondesan, and S. H. Simon, Structure of edge-state inner products in the fractional quantum Hall effect, *Physical Review B* **97**, 155108 (2018).

[56] J. von Delft and H. Schoeller, Bosonization for beginners — refermionization for experts, *Annalen der Physik* **510**, 225 (1998).

[57] L. Winter and O. Zilberberg, in preparation.

[58] F. E. Camino, W. Zhou, and V. J. Goldman, Transport in the Laughlin quasiparticle interferometer: Evidence for topological protection in an anyonic qubit, *Physical Review B* **74**, 115301 (2006).

[59] C. Lin, M. Hashisaka, T. Akiho, K. Muraki, and T. Fujisawa, Quantized charge fractionalization at quantum Hall Y junctions in the disorder dominated regime, Na-

ture Communications **12**, 131 (2021).

[60] M. P. Röösli, M. Hug, G. Nicolí, P. Märki, C. Reichenbacher, B. Rosenow, W. Wegscheider, T. Ihn, and K. Ensslin, Characterization of quasiparticle tunneling in a quantum dot from temperature dependent transport in the integer and fractional quantum Hall regime (2021), arxiv:2112.11935 [cond-mat].

[61] G. Giuliani and G. Vignale, *Quantum Theory of the Electron Liquid* (Cambridge University Press, Cambridge, 2005).

[62] H. Bruus and K. Flensberg, *Many-Body Quantum Theory in Condensed Matter Physics* (Oxford Graduate Texts, 2004).

[63] S. Franke-Arnold, S. M. Barnett, E. Yao, J. Leach, J. Courtial, and M. Padgett, Uncertainty principle for angular position and angular momentum, *New Journal of Physics* **6**, 103 (2004).

[64] G. Jarc, S. Y. Mathengatttil, A. Montanaro, F. Giusti, E. M. Rigoni, F. Fassoli, S. Winnerl, S. D. Zilio, D. Mihailovic, P. Prelovšek, M. Eckstein, and D. Fausti, Cavity control of the metal-to-insulator transition in 1T-TaS<sub>2</sub> (2022), 2210.02346 [cond-mat].

# Supplemental Material for “Fractional quantum Hall edge polaritons”

Authors: Lucas Winter, Oded Zilberberg

Affiliation: Fachbereich Physik, Universität Konstanz, DE-78457 Konstanz, Germany

Date: August 24, 2023

## Short recap on bulk-edge correspondence in the FQHE for Laughlin fractions

In this section, we provide a relevant pedagogical overview of the bulk-edge correspondence in the fractional quantum Hall effect (FQHE) for Laughlin fractions based on Refs. [S1–S4]. First, we introduce the bulk-edge correspondence using qualitative arguments in Sec. . Then, in Sec. , we provide an overview on how to explicitly derive the plasmon wavefunctions from the chiral Luttinger liquid ( $\chi$ LL) edge theory.

### Pedagogical introduction to the bulk-edge correspondence

As discussed in the main text, the fractional quantum Hall droplet hosts plasmonic excitations on the edge of the system. When a plasmonic excitation deforms the edge of the FQHE droplet, it affects the behavior of the electrons in the bulk due to the droplet’s incompressibility and conservation of current [S1, S2]. As a result, it is reasonable to assume that each edge excitation is associated with a bulk wavefunction, which is expected to be similar to the Laughlin wavefunction. In Section , we will explicitly derive the form of this wavefunction using arguments from conformal field theory (CFT). In this section, we will provide some qualitative arguments what these wavefunctions should look like.

There are three conditions that potential bulk representations  $\Psi_l$  of a plasmonic edge excitation  $b_l^\dagger$  should satisfy [S2]

1. The edge excitations must be gapless in the absence of a confinement potential.
2. The edge excitation  $b_l^\dagger$  should possess  $m$  quanta of angular momentum more than the Laughlin ground state.
3. The degeneracy in the spectrum of the edge excitations should be the same as that of the bulk wavefunctions  $\Psi_l$ .

Multiplying the Laughlin wavefunction  $\Psi_0$  with any symmetric polynomial  $s(z_1, \dots, z_n)$  of the electron positions  $z_i$  increases the size of the droplet but keeps the energy at zero. Therefore, the wavefunction must have the general form  $\Psi_l = s(\{z_j\})\Psi_0$  to fulfill the first condition. To satisfy the second condition that the wavefunction possesses the appropriate angular momentum, we can choose the symmetric polynomial  $s(\{z_j\}) = p_l = \sum_k z_j^l$ . Multiplying with a symmetric polynomial  $p_l$  increases the total angular momentum  $m_0$  of the state by  $m$  units  $m_{\text{tot}} = m_0 + m$  [S5]. As a result, the total wavefunction is given by [S3]

$$\Psi_l = p_l \cdot \Psi_0 = \sum_i z_i^l \cdot \Psi_0 = \left( \sum_i z_i^l \right) \cdot \prod_{j < k} (z_j - z_k)^{1/\nu} \prod_k e^{-\frac{1}{4} |z_k|^2}, \quad (\text{SI.1})$$

where we inserted the definition of the Laughlin ground state for the filling fraction  $1/\nu$ . We now need to check if the wavefunctions (SI.1) have the same degeneracy structure as the edge excitations, i.e., that they fulfill the third condition. In this case, it makes sense to assume a quadratic confinement potential that gives the energy  $\hbar\omega_p m$  to the edge modes according to their angular momentum  $m$ . This means that multiplying the Laughlin wavefunction with a symmetric polynomial no longer keeps the energy at zero. To obtain a state with energy  $\hbar\omega_p$ , we can act with  $b_1^\dagger$  on the edge vacuum state or multiply the Laughlin wavefunction with  $p_1$ . This implies that the degeneracy of this first excited state in both the bulk and edge Hilbert spaces is reduced to one. For reaching the  $m_{\text{tot}} = 2$  state, we can act with  $b_1^{\dagger 2}$ ,  $b_1^\dagger$  or multiply the wavefunction with  $p_2$  or  $p_1^2$ , implying that the degeneracy is two [S1, S3]. The general degeneracy structure is summarized in table I.

$m$	1	2	3	...
edge	$b_1^\dagger$	$b_1^\dagger b_1^\dagger$ , $b_2^\dagger$	$b_1^\dagger b_1^\dagger b_2^\dagger$ , $b_1^\dagger$	...
bulk	$\Updownarrow$	$\Updownarrow$	$\Updownarrow$	
degeneracy	$p_1$	$p_1^2$ , $p_2$	$p_1^3$ , $p_1 p_2$ , $p_3$	...
	1	2	3	...

Table I. The edge excitation creation operators and bulk symmetric polynomials combinations necessary to generate a state with a total angular momentum of  $m$ .

The degeneracy structure of the bulk wavefunction is identical to the degeneracy structure of the edge surface waves. There is no analytical proof that the edge states generate the entire Kac-Moody algebra, but the statement has been checked numerically to high precision [S4, S5]. We can conclude that the bulk wavefunctions  $p_1 \cdot \Psi_0$  have similar properties as the edge excitations  $b_i^\dagger$ . This relationship between bulk wavefunctions and correlators on the edge is formalized in Chern-Simons conformal field theory (CFT) [S6–S8].

### Deriving the plasmon wavefunctions using the bulk-edge correspondence

We will now present a comprehensive summary of the CFT methods used to derive the the bulk-edge correspondence following Refs. [S2, S4, S6–S8]. Unlike the Composite Fermion theory, the Chern-Simons theories do not provide a microscopic explanation of the FQHE in terms of probability distributions for individual electrons. Instead, by applying general arguments based on charge conservation and allowed terms in the low-energy limit Lagrangian, CFT identifies a small set of degrees of freedom that can emerge from the complex interactions of many electrons. These effective degrees of freedom describe the low-energy dynamics and long-range order of the FQHE state. Thus, CFT is well-suited for formulating the topological properties of FQHE states in a clear and concise manner [S2]. While CFT is a rich mathematical topic, for this text it is sufficient to see CFT simply as a collection of helpful operators for building FQHE wavefunctions.

The bulk-edge correspondence is a direct result of the quantization of Chern-Simons theories. The Chern-Simons theory describing the quantum hall state is essentially  $3 = 2 + 1$  dimensional. If we cut the CFT in a “time-like” ( $1 + 1$  dimensional) slice, we acquire the CFT of the quantum hall edge. If we cut the CFT at a fixed time in a “space-like” ( $2 + 0$  dimensional) slice, we obtain a CFT describing the ground state. This fact is called the bulk-edge correspondence [S9].

First, we recall some fundamental definitions in the  $\chi$ LL theory of the fractional quantum Hall effect. One important quantity is the edge electron field operator  $\Psi(x)$  destroying one electron at the position  $x$  on the edge. The electron field operator  $\Psi(x)$  can be expressed using the bosonic field  $\phi(x)$  representing the edge plasmons [S10].

$$\Psi(x) \propto e^{-i\frac{1}{\nu}\phi(x)}, \quad (\text{SI.2})$$

where  $\phi(x)$  is related to the edge electron density via  $\rho(x) = \frac{1}{2\pi}\partial_x\phi(x)$ , and can be written using the plasmonic operators on the edge as

$$\phi(x) = -\sqrt{\frac{2\pi\nu}{L}} \sum_{k>0} \frac{1}{\sqrt{k}} \left( e^{-ikx} b_k^\dagger + e^{ikx} b_k \right) e^{-ak/2}, \quad (\text{SI.3})$$

where  $k \in \mathbb{N}$   $L$  is the edge circumference, and  $a$  is the cutoff of the theory.

We illustrate the inner working of constructing wavefunctions using CFT by constructing the edge wavefunctions (SI.1) introduced in Sec. using qualitative arguments. To obtain the wavefunctions, we need to apply a rotation to the time dimension to map the  $1 + 1$  dimensional Lorentzian slice to a  $2 + 0$  dimensional Euclidean space. The mapping can be achieved by Wick rotating the time dimension [S3]

$$w = \frac{2\pi}{L}x_{\text{edge}} + it, \quad w^* = \frac{2\pi}{L}x - it. \quad (\text{SI.4})$$

We can now complete the mapping by considering the complex electron position  $z = e^{-iw} = e^t e^{-i\frac{2\pi}{L}x_{\text{edge}}}$ . We can imagine this mapping in the following way. The time-like slice of the CFT (edge) lives on a cylinder. The circumference of the cylinder, represents the edge at equal time and the vertical direction is the time dimension; see Fig. 1. The bulk is represented by a disc at equal time  $t$ . The mapping (SI.4) now maps a point from the edge of the cylinder to the bulk. A point at  $t = -\infty$  is mapped to the center of the disc [S2].

Applying the Wick rotation (SI.4) to the definition of the bosonic field (SI.3) yields

$$\phi(z) = \phi_0 - ib_0 \ln(z) - \sqrt{\nu} \sum_{l>0} \frac{1}{\sqrt{l}} \left( b_l^\dagger z^{-l} + b_l z^l \right). \quad (\text{SI.5})$$

Here, we have introduced the zero mode of the boson field  $\phi_0$  and  $b_0$  that maintain  $[\phi_0, b_0] = i$  [S2]. We have neglected the zero mode when considering the edge, because it decouples from the edge dynamics and is therefore irrelevant [S2]. Using Eq. (SI.5) it is possible to show that  $\langle \phi(z) \phi(w) \rangle = -\ln(z-w)$ . We wick rotate the electron field operator on the edge  $\Psi(x, t)$  [cf. Eq. (SI.2)], giving rise to the electron field operator of the bulk  $\Psi(z)$

$$\Psi(z) =: e^{i \frac{1}{\nu} \phi(z)} :. \quad (\text{SI.6})$$

where  $: : :$  denotes normal ordering.

For calculating the electron correlator, we need one more aspect. In the plasma analogy of the Laughlin wavefunction, there is a fixed background positive charge density that neutralizes the negative charge of the electrons. This positive charge background is essential for maintaining the charge neutrality of the system and ensuring that the correlator defining the Laughlin wavefunction does not vanish [S9]. The background charge operator is given by [S11]

$$\mathcal{O} = \exp \left( - \frac{i}{2\pi l_B^2} \int dz \phi(z) \right). \quad (\text{SI.7})$$

We can now compute the bulk electron wavefunction by evaluating the CFT correlator over the electron annihilation operators  $\Psi(z)$  (SI.6) and the background charge operator  $\mathcal{O}$  (SI.7) by

$$\left\langle \prod_j \Psi(z_j) \mathcal{O} \right\rangle = \exp \left( - \frac{1}{\nu} \sum_{j < k} \langle \phi(z_j) \phi(z_k) \rangle \right) \exp \left( \sum_k -\frac{1}{2\pi l_B^2 \nu} \int dz \langle \phi(z_k) \phi(z) \rangle \right). \quad (\text{SI.8})$$

Here, we used the fact that the correlator over a free boson field is given [S12]

$$\langle 0 | : e^{A_1} :: e^{A_2} : \cdots : e^{A_n} : | 0 \rangle = \exp \left( \sum_{j < k} \langle 0 | A_j A_k | 0 \rangle \right). \quad (\text{SI.9})$$

We can substitute the correlator  $\langle \phi(z_j) \phi(z_k) \rangle = -\ln(z_j - z_k)$  into Eq. (SI.8). Regarding the integral in Eq. (SI.8) the imaginary part can be undone using a gauge transform. The real part results in the Gaussian factor in the Laughlin wavefunction. In total we obtain [S2]

$$\left\langle \prod_j \Psi(z_j) \mathcal{O} \right\rangle = \prod_{j < k} (z_j - z_k)^{1/\nu} e^{-\frac{1}{4l_B^2} \sum_k |z_k|^2}. \quad (\text{SI.10})$$

This shows that the Laughlin wavefunction can be obtained from CFT correlators (SI.10). Consequently, by using the bulk-edge correspondence, we can derive the complete wavefunction in the bulk with just the understanding of how electrons behave on the edge. Consequently, it is possible to achieve a comprehensive topological classification of the bulk by solely relying on the edge.

We can also compute the wavefunctions of different excitations, such as quasiholes or edge plasmons, by inserting the associated operators into the correlator in Eq. (SI.8). For example, it is possible to obtain the quasihole wavefunction by inserting the operator  $e^{i\sqrt{\nu}\phi(\eta)}$ . Similarly, by inserting the operator  $b_l$  into the correlator (SI.10), it is possible to obtain the bulk wavefunction of the edge excitations [S2, S4]. For the derivation, we follow Ref. [S2]. To obtain the plasmon wavefunction, we need to insert  $b_l$  into the correlator (SI.10)

$$\Psi_l = \left\langle b_l \prod_j : e^{i \frac{1}{\nu} \phi(z_j)} : \mathcal{O} \right\rangle. \quad (\text{SI.11})$$

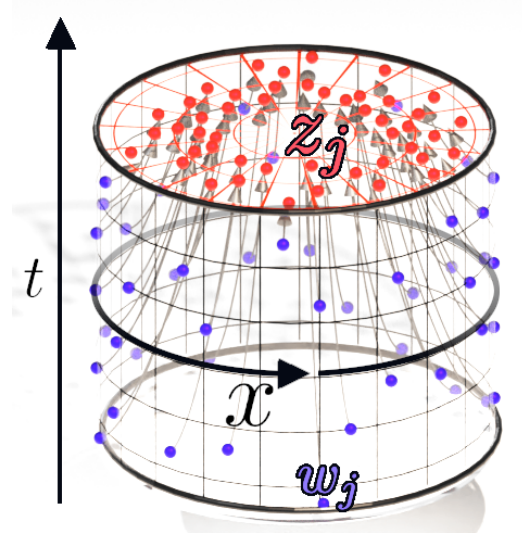


Figure 1. *The state-operator map.* The surface of the cylinder corresponds to the  $1 + 1$ -dimensional slice of the Chern-Simons CFT. The surface of the cylinder is parametrized by  $x$ , the position on the edge of the Hall droplet, and time  $t$ . The disk inside the cylinder represents the  $2 + 0$ -dimensional bulk CFT. The disk is parametrized by the complex variable  $z$  representing the complex electron position in space. By utilizing the state-operator map, a blue point located at  $w_j = \frac{2\pi}{L}x + it$  is projected onto the red disk representing the bulk at  $z_j = x_j + iy_j$ . Points at the beginning of time,  $t = -\infty$ , are mapped to the center of the disk.

If we slide the operator  $b_l$  all the way to the right side of the correlator (SI.11) we annihilate the vacuum. During this process, we have to keep in mind that it does not commute with the vertex operators as

$$[b_l, e^{i\frac{1}{\nu}\phi(z_j)}] = e^{i\frac{1}{\nu}\phi(z_j)} \left[ b_l, -\sum_{l>0} \frac{1}{\sqrt{\nu l}} (b_l^\dagger z^{-l} + b_l z^l) \right] \quad (\text{SI.12})$$

$$= \frac{1}{\sqrt{\nu}} \frac{z^l}{\sqrt{l}} \cdot e^{i\frac{1}{\nu}\phi(z_j)}. \quad (\text{SI.13})$$

However, this implies that the correlator takes the following form

$$\Psi_l = \left\langle b_l \prod_j : e^{i\frac{1}{\nu}\phi(z_j)} : \mathcal{O} \right\rangle = \frac{1}{\sqrt{\nu l}} \sum_j z_j^l \cdot \prod_{j < k} (z_j - z_k)^{1/\nu} e^{-\frac{1}{4t_B^2} \sum_k |z_k|^2}. \quad (\text{SI.14})$$

This is exactly the same form as Eq. (SI.1).

In summary, using the bulk-edge correspondance it is possible to construct the bulk wavefunction of the Laughlin states. This is the case because bulk and edge are described by a space-like  $2 + 0$  dimensional and a time-like  $1 + 1$  dimensional slice respectively of the same underlying CFT. Using Wick rotation (SI.4) one can switch between the different slices [S13].

## Gauge transforms to express the light-matter coupling Hamiltonian in terms of Laughlin wavefunctions

To compute the matrix elements with the Laughlin wavefunctions in the main text, it is vital to express both the Hamiltonian and the cavity vector potential in an appropriate gauge. This means that we need to write the cavity vector potential as a holomorphic function, as the Laughlin wavefunctions also represent holomorphic functions. We will discuss this procedure in section . Next, it is advantageous to express the light-matter coupling term in the Hamiltonian as a functions of the electron positions instead of momenta. To achieve this, we will apply the dipole gauge discussed in section .

### Projecting the vector potential into the lowest Landau Level

In the main body, we explored the derivation of the light-matter coupling Hamiltonian specifically for the mode profile described in Eq. (2) in the main text. However, it is important to note that the angular momentum of light can be represented by various mode profiles, such as Laguerre-Gaussian modes, Bessel modes, or hypergeometric Gaussian modes[S14, S15]. In this section we demonstrate how to express an arbitrary vector potential such that it lies in the lowest Landau level.

In general, the vector potential is a three-dimensional vector field, represented by  $\mathbf{A}(x, y, z)$ , that depends on all spatial coordinates. However, since the electrons of the fractional quantum Hall effect can only move in the 2DEG, which is parameterized by  $(x, y)$ , we must project the vector potential. This involves setting  $z = 0$  and neglecting the  $A_z$  component, as this component exerts an out-of-plane force on the electrons. Consequently, the vector potential of a single mode that carries a clearly defined angular momentum of light may typically be expressed in this way.

$$\mathbf{A}(\mathbf{r}) = A(z)\boldsymbol{\epsilon} + A^*(z)\boldsymbol{\epsilon}^* . \quad (\text{SII.16})$$

The FQH wavefunctions are expressed as holomorphic functions of the electron position  $z = x + iy$ . To project the light-matter coupling Hamiltonian  $H_{\text{int}} = \frac{e}{\hbar} \mathbf{E} \cdot \mathbf{r}$  on the plasmon subspace, it is convenient to express the mode profile  $A(z)$  itself as a holomorphic function of the complex variable  $z$ . This can be achieved by a gauge transform  $\chi$  under which the vector potential  $\mathbf{A}$  and the scalar potential  $V$  transform like

$$\mathbf{A} \rightarrow \mathbf{A} + \nabla\chi = \tilde{\mathbf{A}} , \quad (\text{SII.17})$$

$$V \rightarrow V - \partial_t\chi = \tilde{V} , \quad (\text{SII.18})$$

where we take  $\chi(x, y)$  as a real valued function. When considering  $\boldsymbol{\epsilon} = (1, i, 0)/\sqrt{2}$  in the case of circular polarization, we obtain

$$\mathbf{A} = \frac{1}{\sqrt{2}} \begin{pmatrix} \Re\{A(z)\} \\ -\Im\{A(z)\} \end{pmatrix} \rightarrow \mathbf{A} + \nabla\chi = \frac{1}{\sqrt{2}} \begin{pmatrix} \Re\{A(z) + \partial_x\chi\} \\ -\Im\{A(z) - i\partial_y\chi\} \end{pmatrix} . \quad (\text{SII.19})$$

This implies that under a gauge transformation,  $A(z)$  transforms as  $A(z) \rightarrow A(z) + \partial_x\chi - i\partial_y\chi$ . Now, let's consider a complex-valued scalar  $\chi(z = x + iy)$ , where  $2d_z\chi = \partial_x\chi(x, y) - i\partial_y\chi(x, y)$ . By introducing a complex  $\chi(z)$ , we can express the gauge transformation simply as  $A(z) = A(z) + d_z\chi(z)$ .

Our objective now is to determine a gauge transformation  $\chi(z)$  such that  $A_{\text{hol}} = A(z) + d_z\chi$  is holomorphic. According to the Cauchy-Riemann conditions,  $A_{\text{hol}}$  should not depend on the antiholomorphic variable, i.e.,  $d_{(z^*)}A(z) = 0$ . This implies that  $A_{\text{hol}}$  must satisfy the differential equation:

$$\frac{d}{dz^*}\tilde{\mathbf{A}} = \frac{d}{dz^*} \left( \mathbf{A} + \frac{d}{dz}\chi \right) = 0 , \quad (\text{SII.20})$$

$$\frac{d^2\chi}{(dz)(dz^*)} = -\frac{dA(z)}{dz^*} . \quad (\text{SII.21})$$

In turn, this implies that by solving the differential Eq. (SII.21), we can determine the suitable gauge transformation that renders the mode profile holomorphic. Equation (SII.21) bears similarity to the Poisson equation  $\Delta\chi = -\nabla \cdot A$ , which one must solve to express a vector potential in the Coulomb gauge [S16].

In polar coordinates  $z = re^{i\varphi}$  Eq. (SII.21) can be written as

$$\frac{e^{-i\phi}}{2} \left( \frac{1}{r^2} \partial_\phi^2 + \frac{1}{r} \partial_r + \partial_r^2 \right) \chi = - \left( \partial_r - \frac{1}{ir} \partial_\phi \right) A(r, \varphi) . \quad (\text{SII.22})$$

In the special case that the mode profile  $A(z)$  is an eigenstate of the angular momentum operator  $L_z = -i\hbar\partial_\varphi$ , we can write it as  $A(z) = A(r)e^{im\varphi}$ . In this case, we can use the Ansatz  $\chi(r, \varphi) = \chi(r)e^{il\varphi}$  where  $l = m + 1$ . By solving the differential equation

$$\frac{1}{2} \left( \frac{l^2}{r^2} \chi - \frac{1}{r} \partial_r \chi - \partial_r^2 \chi \right) = \left( \partial_r + \frac{l-1}{r} \right) A(r) , \quad (\text{SII.23})$$

we can determine the radial profile of the gauge transform  $\chi$ .

After obtaining the holomorphic mode profile  $\tilde{A}(z)$  corresponding to  $\tilde{\mathbf{A}} = \tilde{A}(z)\mathbf{\epsilon} + \tilde{A}(z)^*\mathbf{\epsilon}^*$ , we can now quantize it in terms of angular momentum modes. As the plasmon wavefunctions are holomorphic, it is reasonable to apply holomorphic quantization. This means that we express the vector potential as a Taylor series in the holomorphic variable  $z$

$$A(z) = \sum_{m=0} A_{0,m} z^m a_m , \quad (\text{SII.24})$$

where the Taylor coefficients  $A_{0,m}$  are given by  $A_{0,m} = \frac{d^m A(z)}{dz^m}|_{z=0}$  and  $a_m$  represents a complex amplitude. Using  $l = m + 1$  and  $A_{0,l} = A_{0,m+1}$ , the total vector potential then takes the form

$$\tilde{\mathbf{A}} = \sum_{l>0} A_{0,l} z^l a_l + A_{0,l}^*(z^*)^{l-1} a_l^\dagger . \quad (\text{SII.25})$$

The quantization is complete when promoting  $a_l$  and  $a_l^\dagger$  to quantum mechanical operators with  $[a_l, a_{l'}^\dagger] = \delta_{l,l'}$  and  $[a_l, a_{l'}] = [a_l^\dagger, a_{l'}^\dagger] = 0$ . Then Eq. (SII.25) has the same form as the vector potential presented in the main text (2).

### The quantum Hall Hamiltonian in the Dipole gauge

In the main text, we discussed the application of the dipole gauge to the bulk FQH Hamiltonian  $H_c$  [cf. Eq. (1) in the main text] in order to accurately consider the cavity's perturbation. In this section, we will perform a complete calculation for implementing the dipole gauge and explore all relevant terms, including those specific to the ultrastrong coupling regime ( $g_{\text{Rabi}} > \omega_c$ ), which were not covered previously. For simplicity, we will not explicitly include the Hamiltonian terms  $V_{\text{int}}$  and  $V_{\text{conf}}$  as they are not crucial for the subsequent analysis.

We start by expanding the Hamiltonian in the Coulomb gauge [cf. Eq. (1) in the main text] to obtain

$$H = \underbrace{\frac{1}{2m_e} \boldsymbol{\pi}^2}_{=H_L} - \underbrace{\frac{e}{2m_e} (\boldsymbol{\pi} \cdot \mathbf{A} + \mathbf{A} \cdot \boldsymbol{\pi})}_{=H_{\text{int}}} + \underbrace{\frac{e^2}{2m_e} \mathbf{A}^2}_{=H_{\text{Dia}}} + \underbrace{\sum_{l>0} \hbar \omega_{c,l} a_l^\dagger a_l}_{=H_C} . \quad (\text{SII.26})$$

Here, and in the following, we will use the canonical momentum  $\boldsymbol{\pi} = \mathbf{p} - e\mathbf{A}_{\text{ext}}$ . The term  $H_L$  captures all single-electron contributions,  $H_{\text{int}}$  denotes the light-matter coupling term in the Coulomb gauge, and  $H_C + H_{\text{Dia}}$  denotes the Hamiltonian of the cavity.

To apply the dipole gauge, we utilize a unitary transformation  $U$  on the bulk Hamiltonian (SII.26), yielding  $H_D = U H_C U^\dagger$ . The objective is to express the light-matter coupling term, which involves both photon and electron operators, in terms of the electron position  $\mathbf{r}$  rather than the momentum  $\mathbf{p}$ . For the cavity vector potential given in Eq. (2) in the main text, this transformation can be achieved using the operator

$$U = \exp \left( \sum_{l>0} G_l \right) = \exp \left( - \frac{i}{\hbar} \sum_{l>0} e \frac{\mathbf{r} \cdot \mathbf{A}_l}{l} \right) , \quad (\text{SII.27})$$

where  $G_l = -\frac{ie}{l\hbar} \mathbf{A}_l \cdot \mathbf{r} = \frac{ie}{l\hbar\sqrt{2}} R A_{0,l} (z^l a_l + (z^*)^l a_l^\dagger)$ .

To apply the operator  $U$  [cf. Eq. (SII.27)], the Baker-Campbell-Hausdorff lemma is useful:  $e^B A e^{-B} = A + [B, A] + \frac{1}{2!} [B, [B, A]] + \dots$ . Now, let us compute the fundamental commutators necessary to apply the Baker-Campbell-Hausdorff lemma. The operator  $G_l$  generally commutes with position operators. However, the commutator with the electron canonical momenta  $\pi_x$  and  $\pi_y$  are not vanishing, as

$$[G_l, \pi_x] = eA_{0,l}(z^{l-1}a_l + (z^*)^{l-1}a_l^\dagger) = eA_x , \quad (\text{SII.28})$$

$$[G_l, \pi_y] = eA_{0,l}i(z^{l-1}a_l - (z^*)^{l-1}a_l^\dagger) = eA_y , \quad (\text{SII.29})$$

and  $G_l$  does not commute with the components of the cavity vector potential. Here, we have

$$[G_l, A_{x,l'}] = \frac{eA_{0,l}^2}{l\hbar}y|z|^{2l-1}\delta_{l,l'} , \quad (\text{SII.30})$$

$$[G_l, A_{y,l'}] = -\frac{eA_{0,l}^2}{l\hbar}x|z|^{2l-1}\delta_{l,l'} . \quad (\text{SII.31})$$

Using the fundamental commutators (SII.28), (SII.29), (SII.30), and (SII.31), along with the Baker-Campbell-Hausdorff lemma, we can apply the dipole gauge to the various terms in the Hamiltonian (SII.26). We begin with  $H_L$ :

$$\begin{aligned} UH_LU^\dagger &= \frac{\pi^2}{2m_e} + \sum_{l>0} [G_l, \frac{\pi^2}{2m_e}] + \sum_{l,l'>0} \frac{1}{2} [G_l, [G_{l'}, \frac{\pi^2}{2m_e}]] \\ &= \frac{\pi^2}{2m_e} + \frac{e}{2m_e}(\boldsymbol{\pi} \cdot \mathbf{A} + \mathbf{A} \cdot \boldsymbol{\pi}) + \frac{e^2}{2m_e}\mathbf{A}^2 + \frac{e^2A_0^2}{m_e\hbar}\Upsilon(|z|)(\boldsymbol{\pi} \times \mathbf{r}) \cdot \hat{\mathbf{e}}_z . \end{aligned} \quad (\text{SII.32})$$

where we used  $A_x = \sum_{l>0} A_{x,l}$  and  $A_x^2 = \sum_{l>0} A_{x,l} \cdot \sum_{l'>0} A_{x,l'}$ . Additionally, we defined

$$\Upsilon(|z|) = \frac{1}{A_0^2|z|} \sum_{l>0} \frac{A_{0,l}^2}{l}|z|^{2l} = \frac{1}{|z|} \int_{|z'|\leq|z|} dz' |A(z')|^2 , \quad (\text{SII.33})$$

with the normalization constant  $A_0^2 = \int dz |A(z)|^2$ . Please note that  $\Upsilon(|z|)$  is a monotonously increasing function with  $\Upsilon(0) = 0$  and  $\Upsilon(1) = 1$ .

Next, we express  $H_{\text{int}}$  in the dipole gauge:

$$UH_{\text{int}}U^\dagger = -\frac{e}{m_e}(\boldsymbol{\pi} \cdot \mathbf{A} + \mathbf{A} \cdot \boldsymbol{\pi}) - \frac{e^2}{m_e}\mathbf{A}^2 - \frac{2e^2A_0^2}{m_e\hbar}\Upsilon(|z|)(\boldsymbol{\pi} \times \mathbf{r}) \cdot \hat{\mathbf{e}}_z . \quad (\text{SII.34})$$

The diammagnetic term  $H_{\text{Dia}}$  in the the dipole gauge reads

$$\begin{aligned} UH_{\text{Dia}}U^\dagger &= \frac{e^2}{2m_e}\mathbf{A}^2 + \sum_{l>0} [G_l, \frac{e^2}{2m_e}\mathbf{A}^2] + \sum_{l,l'>0} \frac{1}{2} [G_l, [G_{l'}, \frac{e^2}{2m_e}\mathbf{A}^2]] \\ &= \frac{e^2}{2m_e}\mathbf{A}^2 + \frac{e^3A_0^2}{m_e\hbar}\Upsilon(|z|)(\mathbf{A} \times \mathbf{r}) \cdot \hat{\mathbf{e}}_z + \frac{2e^4A_0^4}{m_e\hbar^2}\Upsilon^2(|z|)\mathbf{r}^2 . \end{aligned} \quad (\text{SII.35})$$

Last, we calculate the commutator with the cavity  $H_c = \sum_{l>0} \hbar\omega_c a^\dagger a_l$ . Using the form of the vector potential [cf. Eq. (2) in the main text], we obtain

$$UH_CU^\dagger = \sum_l \frac{1}{l}\mathbf{E}_l \cdot \mathbf{r} + \frac{e^2\omega_c A_0^2}{2\hbar}\Upsilon(|z|)(x^2 + y^2) , \quad (\text{SII.36})$$

where we have defined  $\mathbf{E} = -i \sum_{l>0} \omega_{c,l} A_{0,l} (\epsilon z^l a_l - \epsilon^* (z^*)^l a_l^\dagger)$ .

We can now combine the individual transformed terms (SII.32), (SII.34), (SII.35) and (SII.36), to obtain

$$H_D = H_L + H_C + \underbrace{D(|z|)\mathbf{r}^2}_{=H_{\text{conf}}} + \underbrace{\gamma(|z|)\hat{\mathbf{e}}_z \cdot (\boldsymbol{\pi} \times \mathbf{r})}_{=H_{\text{prec}}} + e \underbrace{\sum_{l>0} \frac{1}{l}\mathbf{E}_l \cdot \mathbf{r}}_{=H_{\text{int,D}}} \underbrace{-e\gamma(|z|)\hat{\mathbf{e}}_z \cdot (\mathbf{r} \times \mathbf{A})}_{=H_{\text{int,2}}} , \quad (\text{SII.37})$$

where  $D(|z|) = 1/2 (e^2 \omega_c A_0^2 / \hbar \Upsilon(|z|) + 2e^4 / (m \hbar^2 A_0^4) \Upsilon(|z|)^2)$ , and  $\gamma(|z|) = e^2 A_0^2 / (m_e \hbar) \Upsilon(|z|)$ .

We can now determine all of the additional terms that are relevant in the strong coupling regime. For this purpose, we compare the energy of each additional term with the energy scale of the light-matter coupling interaction  $H_{\text{int}} = e \sum_{l>0} \mathbf{E} \cdot \mathbf{r} / l$ . To this end, we can assume the position is on the order of the magnetic length  $|\mathbf{r}| \propto l_B = \sqrt{\hbar/(eB)}$  and  $|\boldsymbol{\pi}| \propto \hbar/l_B = \sqrt{\hbar e B}$ . Please note that the Rabi frequency in the system is given by  $g_{\text{Rabi}} = \frac{e}{\hbar} A_0 \sqrt{(\hbar \omega_{\text{cyc}})/(2m_e)}$  with the cyclotron frequency  $\omega_{\text{cyc}} = (eB)/m_e$  [S17].

First, we look at the confining potential term  $V_{\text{conf}}$  in Eq. (SII.37). It lifts the angular momentum degeneracy particularly at the edges, and can shift the cyclotron frequency. Its energy compared to the light-matter coupling Hamiltonian  $H_{\text{int}}$  is

$$\frac{|V_{\text{conf}}|}{|H_{\text{int}}|} \leq \sqrt{2} \frac{g_{\text{Rabi}}}{\omega_{\text{cyc}}} \left( 1 + 4 \frac{g_{\text{Rabi}}^2}{\omega_{\text{cyc}} \omega_c} \right). \quad (\text{SII.38})$$

Here, we approximated  $\Upsilon(|z|) \leq \Upsilon(1) = 1$ ; cf. Eq. (SII.33). This shows that in the ultrastrong coupling regime  $g_{\text{Rabi}} < \omega_{\text{cyc}}$ , the confinement potential has only a small effect and can thus be neglected.

Next, we look at the term  $H_{\text{prec}}$ . This is a precession term leading to a shift in the cyclotron frequency. Compared with the interaction Hamiltonian, we have

$$\frac{|H_{\text{prec}}|}{|H_{\text{int}}|} \leq \frac{g_{\text{Rabi}}}{\omega_c}. \quad (\text{SII.39})$$

As the cavity frequency for coupling to plasmons,  $\omega_c$ , is significantly lower than the cyclotron frequency,  $\omega_{\text{cyc}}$ , it cannot be completely neglected in the strong coupling regime. However, its presence primarily affects the single-electron spectrum, resulting in quantitative modifications rather than qualitative ones. In the bulk, it introduces corrections to the cyclotron frequency, while at the edge, it leads to additional corrections to the plasmon drift velocity.

Last, let us examine the second light-matter coupling term. Here, we find

$$\frac{|H_{\text{int},2}|}{|H_{\text{int}}|} \leq \frac{g_{\text{Rabi}}^2}{\omega_c \omega_{\text{cyc}}}. \quad (\text{SII.40})$$

Once more, we observe that this term is not relevant in the strong coupling regime, where  $g_{\text{Rabi}} \ll \omega_{\text{cyc}}$ .

In conclusion, in the strong coupling regime, we can express the Hamiltonian in the dipole gauge as follows:

$$H_D = \frac{\pi^2}{2m_e} + \hbar \omega_c \sum_{l>0} a_l^\dagger a_l + e \sum_{l>0} \frac{1}{l} \mathbf{E}_l \cdot \mathbf{r}. \quad (\text{SII.41})$$

This Hamiltonian (SII.41) is also presented in the main text as Eq. (3).

### Symmetry constraints to plasmon-photon coupling

In the main text, we argued, based on rotational symmetry, that the total angular momentum of photons and plasmons should be conserved. In this section, we formalize this argument and explicitly show that  $H_D$  [cf. Eq. (SII.27)] commutes with the total angular momentum operator  $L_z = L_{z,e} + L_{z,p}$ , which consists of the electron angular momentum  $L_{z,e}$ , and the photon angular momentum  $L_{z,p}$ .

The photons carry the angular momentum  $l = m+1$  composed of one quantum spin angular momentum (SAM) and  $m$  quanta of orbital angular momentum (OAM). This means that the cavity electric field  $\mathbf{E} = i(E(z)\boldsymbol{\epsilon}a - A^*(z)\boldsymbol{\epsilon}^*a^\dagger)$  has a circular polarization vector  $\boldsymbol{\epsilon} = (1, i, 0)/\sqrt{2}$ , and a mode profile given by  $E(z) = z^m$ .

For the following considerations, we assume that the system is in the strong coupling regime. In the previous section, we discussed that the Hamiltonian in the dipole gauge (SII.37) simplifies to Eq. (SII.41) in the strong coupling regime. Furthermore, we know that both the cavity and the FQH system, conserve angular momentum. Consequently, angular momentum conservation can only be broken by the light-matter coupling term in Eq. (SII.41)

$$H_{\text{int}} = \frac{e}{l} \mathbf{E}_l \cdot \mathbf{r}. \quad (\text{SIII.42})$$

Here, we substituted the expression for the electric field  $\mathbf{E}$  and used the fact that the scalar product between the position and the polarization vector  $\boldsymbol{\epsilon} = (1, i, 0)/\sqrt{2}$ , and the electron position  $\mathbf{r}$  is given by  $\mathbf{r} \cdot \boldsymbol{\epsilon} = Rz/\sqrt{2}$ .

To check whether  $H_{\text{int}}$  (SIII.42) conserves angular momentum, we need the angular momentum operators for the electrons and the cavity photons. Classically, the angular momentum operator for the electrons in the  $z$  direction is given by  $L_{z,e} = \hat{\mathbf{e}}_z \cdot (\mathbf{r} \times \mathbf{p}) = xp_y - yp_x$ . Using canonical quantization,  $L_{z,e}$  can be extended to the quantum regime by replacing the observables with the corresponding position and momentum operators. This yields the following differential operator  $L_{z,e} = -i\hbar(x\partial_y - y\partial_x)$ . Casting the operator in polar coordinates generates the angular momentum operator

$$L_{z,e} = -i\hbar\partial_\varphi . \quad (\text{SIII.43})$$

Thus, we have found the angular momentum operator for the electrons.

For the photons, we can use the fact that they carry  $l = m + 1$  quanta of angular momentum. The total angular momentum of the cavity can then be determined using the number operator

$$L_{z,p} = \hbar a_l^\dagger a_l . \quad (\text{SIII.44})$$

To show angular momentum conservation, we have to show that the total angular momentum operator  $L_z = L_{z,e} + L_{z,p}$ , consisting of the electron angular momentum  $L_{z,e}$  (SIII.43) and photon angular momentum  $L_{z,p}$  (SIII.44), commutes with the interaction Hamiltonian  $H_{\text{int}}$  (SIII.42). Evaluating the commutator yields

$$[L_z, H_{\text{int}}] = \left[ -i\hbar\partial_\varphi, \frac{e}{l} \left( z^l a - (z^*)^l a^\dagger \right) \right] + \left[ \hbar a_l^\dagger a_l, \frac{e}{l} \left( z^l a - (z^*)^l a^\dagger \right) \right] . \quad (\text{SIII.45})$$

We apply the commutators  $[-i\hbar\partial_\varphi, z^l] = \hbar l z^l$ . Then, Eq. (SIII.45) becomes

$$[L_z, H_{\text{int}}] = \hbar e \left( z^l a + (z^*)^l a^\dagger \right) - \hbar e \left( z^l a + (z^*)^l a^\dagger \right) = 0 . \quad (\text{SIII.46})$$

The commutator (SIII.46) shows that the total angular momentum is conserved by the Hamiltonian  $H_D$  (SII.41). This means that as the edge plasmons carry angular momentum, the light-matter coupling term must have the form  $H_{\text{int}} \propto b_l^\dagger a - a^\dagger b_l$  since otherwise the total angular momentum is not conserved. While this does not give information on the coupling strength, symmetry arguments completely determine the mathematical shape of the photon-plasmon Hamiltonian.

Up to this point, we have assumed that the cavity electric field  $\mathbf{E}$  has the same chirality as the plasmon modes. For opposing chiralities, one might expect that rotation invariance breaks down and that the angular momentum is no longer conserved. We can, however, obtain the cavity field with opposite chirality by the symmetry transform  $x \rightarrow x$  and  $y \rightarrow -y$ . This means  $\epsilon \rightarrow \epsilon^*$  and  $E(z) \rightarrow E^*(z)$ . In this case, the interaction Hamiltonian  $H_{\text{int}}$  (SIII.42) becomes

$$H_{\text{int}} = \frac{e}{l} \mathbf{E}_l \cdot \mathbf{r} = \frac{e}{l} \left( (z^*)^l a - z^l a^\dagger \right) . \quad (\text{SIII.47})$$

By computing the commutator of  $H_{\text{int}}$  (SIII.47) with  $L_z$  [cf. Eqs. (SIII.43) and (SIII.44)], we find

$$[L_z, H_{\text{int}}] = 2\hbar e \left( z^l a + (z^*)^l a^\dagger \right) \neq 0 . \quad (\text{SIII.48})$$

The resulting commutator (SIII.48) shows that the total angular momentum is no longer conserved by the electron-photon interaction. This also implies that the total particle number of photons and plasmons is not necessarily conserved any longer.

While for the opposing chirality of the edge waves and cavity photons the sum of the angular momentum of the FQH system and the cavity is not conserved  $L_z = L_{z,e} + L_{z,p}$  (SIII.43), the difference  $\Delta L_z = L_{z,e} - L_{z,p}$  is. Indeed, by evaluating the commutator of  $\Delta L_z$  with  $H_{\text{int}}$  (SIII.47), we find

$$[\Delta L_z, H_{\text{int}}] = \hbar e \left( z^l a + (z^*)^l a^\dagger \right) - \hbar e \left( z^l a + (z^*)^l a^\dagger \right) = 0 . \quad (\text{SIII.49})$$

The fact that the angular momentum difference  $\Delta L$  between cavity and FQH system is conserved (SIII.49) also imposes significant constraints on the photon-plasmon interaction Hamiltonian. It means that if a photon-plasmon interaction increases the angular momentum of the cavity by  $l$  units, it must also increase the angular momentum on the edge by  $l$  units. Therefore, the interaction Hamiltonian consists only of terms of the form  $b_l^\dagger a^\dagger$  or  $b_l a$ .

In summary, if the chirality of the edge waves matches the cavity mode, the total angular momentum  $L_z = L_{z,e} + L_{z,p}$  is conserved (SIII.46). This implies that the light-matter coupling consists of terms of the form  $a^\dagger b_l$  or  $ab_l^\dagger$ . If the chirality of the light field is opposite to the chirality of the edge wave, the angular momentum difference  $\Delta L = L_{z,e} - L_{z,p}$  is conserved (SIII.49). Therefore, the photon-plasmon coupling Hamiltonian can only consist of terms of the form  $a^\dagger b_l^\dagger$  and  $ab_l$ .

### Details on the applied Schrieffer-Wolff transform

In this supplement, we discuss how to analyze the cavity mediated interactions between opposing edges of the  $\chi_{\text{LL}}$  using a Schrieffer-Wolff transform. Initially, the system is described by the Hamiltonian (6) in the main text. In the main text, we use, for brevity, the definition  $b_q = \Theta(q)b_{R,q} + \Theta(-q)b_{L,q}$  and  $b_q^\dagger = \Theta(q)b_{R,q}^\dagger + \Theta(-q)b_{L,q}^\dagger$ , where  $b_{q,R}$  represents a plasmon on the right edge and  $b_{q,L}$  represents a plasmon on the left edge. Here, we will use the operators  $b_{q,L}$  and  $b_{q,R}$  for clarity. The Hamiltonian [cf. Eq. (6) in the main text] reads in this case

$$H = \sum_{q>0} \left[ \underbrace{\hbar v q (b_{R,q}^\dagger b_{R,q} + b_{L,q}^\dagger b_{L,q}) + \hbar \omega_c a_q^\dagger a_q}_{=H_0} + \underbrace{i\hbar g (a_q b_{R,q}^\dagger - a_q^\dagger b_{R,q} + a_q b_{L,q} - a_q^\dagger b_{L,q}^\dagger)}_{=H_{\text{int}}} \right]. \quad (\text{SIV.50})$$

To decouple the cavity from the edge modes, we employ the Schrieffer-Wolff transformation to the Hamiltonian. We seek a unitary transformation that when applied, will perturbatively diagonalize the Hamiltonian up to first order. In other words, the goal is to find an operator  $S$  such that  $[H_0, S] = V$ , where  $H_0$  is the unperturbed Hamiltonian and  $V$  is the perturbation. We can construct the operator  $S$  as

$$S = \sum_{q>0} i g \left[ \frac{1}{\omega_c - v q} (a_q b_{R,q}^\dagger + a_q^\dagger b_{R,q}) - \frac{1}{\omega_c + v q} (a_q b_{L,q} + a_q^\dagger b_{L,q}^\dagger) \right]. \quad (\text{SIV.51})$$

We can now apply the unitary transformation  $H_{\text{eff}} = e^S H e^{-S}$ . Using the Baker-Campbell-Hausdorff lemma  $e^S H e^{-S} = H + [S, H] + \frac{1}{2} [S, [S, H]] + \dots$  and neglecting any terms of second order or higher, we find

$$H_{\text{eff}} = H_0 + [S, V] = H_0 + \sum_{q>0} g^2 \left[ -\frac{1}{\omega_c - qv} b_{R,q}^\dagger b_{R,q} - \frac{1}{\omega_c + vq} b_{L,q}^\dagger b_{L,q} + \frac{\omega_c}{\omega_c^2 - v^2 q^2} (b_{L,q}^\dagger b_{R,q}^\dagger + b_{L,q} b_{R,q}) \right]. \quad (\text{SIV.52})$$

Now, switching back to the plasmon operator definitions used in the main text  $b_q = \Theta(q)b_{R,q} + \Theta(-q)b_{L,q}$  and  $b_q^\dagger = \Theta(q)b_{R,q}^\dagger + \Theta(-q)b_{L,q}^\dagger$ , the effective Hamiltonian can be written in a more compact form as

$$H_{\text{eff}} = \sum_{q \neq 0} \left[ \hbar \left( v_p - \frac{g^2}{|q|} \frac{1}{\omega_c - qv} \right) |q| b_q^\dagger b_q + \hbar \frac{g^2}{|q|} \frac{\omega_c}{\omega_c^2 - v^2 q^2} |q| (b_q^\dagger b_{-q}^\dagger + b_q b_{-q}) \right]. \quad (\text{SIV.53})$$

For convenience, as in the main text, we define  $V_1(q) = -\frac{g^2}{|q|} \frac{1}{\omega_c - qv}$  and  $V_2(q) = -\frac{g^2}{|q|} \frac{\omega_c}{\omega_c^2 - v^2 q^2}$ , giving us the same form as displayed in Eq. (7) in the main text.

### Details on the Conductivity Calculation

Here, we will delve deeper into the process of calculating the conductivity when dealing with a single-mode and a multi-mode cavity within the framework of Luttinger liquid theory for a system described by the effective Hamiltonian [cf. Eq. (7) in the main text]. We will specifically focus on a Luttinger liquid situated between two electrodes. In this configuration, the left electrode sets the chemical potential of the right-movers to  $V_s$ , while the right electrode maintains the chemical potential of the left-movers at zero. Given the electrode position  $x_s$ , we can derive the following potential [S18]

$$V(x) = \begin{cases} V_s \cos(\omega t) & x < x_s \\ 0 & \text{otherwise} \end{cases}. \quad (\text{SV.54})$$

Using Kubo's formula, the conductivity in this setup is generally given by [S18]

$$I = -e \lim_{\omega \rightarrow 0} \int_{-\infty}^0 \chi_{j,n}(x - x', \omega) V_s dx', \quad (\text{SV.55})$$

where  $\chi$  is the current density response function. Here, we will not take into account internal screening effects. The response function itself is given by [S18]

$$\chi = -\frac{ie}{\hbar L} \int \frac{dq}{2\pi} e^{iq(x-x')} \int_0^\infty \langle [j_q(t), n_{-q}(0)] \rangle e^{i(\omega+i\eta)t}. \quad (\text{SV.56})$$

This means that with the substitution  $G_j(q, \omega) = \int_0^\infty dt \langle [j_q(t), n_{-q}(0)] \rangle e^{i(\omega+i\eta)t}$ , we obtain the same form as Eq. (8) in the main text:

$$\sigma = \frac{e^2}{\hbar L} \int_{-\infty}^0 dx' \sum_{q \neq 0} e^{iq(x-x')} G_j(q, \omega). \quad (\text{SV.57})$$

Equation (SV.57) shows that the conductivity can be calculated as the sum over individual current correlation functions. By inserting the density operator  $n_q = \sqrt{\frac{L|q|\nu}{2\pi}}(\beta_q + \beta_{-q}^\dagger)$  and the current operator  $j_q = \sqrt{\frac{L|q|\nu}{2\pi}}v_p \operatorname{sgn}(q)(\beta_q - \beta_{-q}^\dagger)$  into  $G_{j,q}$ , we find

$$G_j(q, \omega) = i \int_0^\infty dt e^{i(\omega+i\eta)t} \langle [j_q(t), n_{-q}(0)] \rangle \quad (\text{SV.58})$$

$$= i \int_0^\infty dt e^{i(\omega+i\eta)t} \frac{Lq}{2\pi} v \nu \langle [\beta_q(t) + \beta_{-q}^\dagger(t), \beta_{-q}(0) - \beta_q^\dagger(0)] \rangle. \quad (\text{SV.59})$$

As  $\beta_q^\dagger(t) = e^{i\omega_q t} \beta_q(0)$ , we find

$$G_j(q, \omega) = i\nu \frac{Lvq}{2\pi} \left( \frac{1}{\omega - v_q|q|} + \frac{1}{\omega + v_{-q}|q|} \right). \quad (\text{SV.60})$$

We will now consider the case of a single and a multimode cavity separately:

### Single mode cavity

In the case of a single-mode cavity, only a single plasmon mode couples to the cavity with wavevector  $q_c = \frac{2\pi}{L}l$ , where  $l$  denotes the angular momentum of the cavity mode. This means that the current correlation functions have the following form

$$\tilde{G}_j(q_c, \omega) = i \frac{Lq_c}{2\pi} v \left( \frac{1}{\omega - v_{q_c}|q_c|} + \frac{1}{\omega + v_{-q_c}|q_c|} \right), \quad (\text{SV.61})$$

$$G(q, \omega) = i \frac{Lq}{2\pi} v \frac{\omega}{\omega^2 - v^2 q^2}. \quad (\text{SV.62})$$

Here  $\tilde{G}(q_c, \omega)$  (SV.61) is the cavity modified plasmon correlation function for  $q = q_c$ , whereas  $G_j(q, \omega)$  (SV.62) is the plasmon correlation function that unaffected by the cavity. We can now calculate the conductivity by inserting  $G_j(q, \omega)$  (SV.61) into the expression for the conductivity [cf. Eq. (8) in the main text]. We obtain

$$\sigma = -\frac{ie\nu}{\hbar L} \lim_{\omega \rightarrow 0} \left( \underbrace{\int_{-\infty}^0 dx' \sum_{q \neq 0} e^{iq(x-x')} G_j(q, \omega)}_{=\sigma_0} + \underbrace{\int_{-\infty}^0 \sum_{q=\pm q_c} e^{iq(x-x')} \left( \tilde{G}(q, \omega) - G(q, \omega) \right)}_{=\tilde{\sigma}} \right). \quad (\text{SV.63})$$

We can now compute the conductivity  $\sigma_0$  (similarly to Ref. [S18]) by moving to the continuum limit

$$\sigma_0 = \frac{e^2}{\hbar L} \lim_{\omega \rightarrow 0} \int_{-\infty}^0 dx' \int dq e^{iq(x-x')} \frac{Lq}{2\pi} v \frac{\omega}{\omega^2 - v^2 q^2}. \quad (\text{SV.64})$$

We evaluate the integral using the residue theorem  $q = \omega/v$ . This will result in (see also Ref. [S18])

$$\sigma_0 = \frac{e^2 \nu}{h}. \quad (\text{SV.65})$$

Now, we calculate  $\tilde{\sigma}$ . In this case, we use  $\lim_{\omega \rightarrow 0} \tilde{G}(q, \omega) = \frac{L}{2\pi} v \operatorname{sgn}(q)(1/v_{-q} - 1/v_q)$  and  $\lim_{\omega \rightarrow 0} G(q, \omega) = 0$  to find

$$\tilde{\sigma} = \frac{e^2 \nu}{\hbar L} \frac{L}{2\pi} \int dx' \left( \frac{1}{v_{-q_c}} - \frac{1}{v_{-q_c}} \right) \cos(q_c(x - x')) = \frac{e^2 \nu}{\hbar} v \left( \frac{1}{v_q} - \frac{1}{v_{-q}} \right) \sin(q_c(x - x')). \quad (\text{SV.66})$$

By combining Eqs. (SV.65) and (SV.66), we find the same form as Eq. (9) in the main text.

### Multimode cavity

For this scenario, we can adopt a continuum description for the summation over  $q$  as seen in Eq. (SV.57). It is important to highlight that a minimum wave vector cutoff, given by  $g(q) = gq^2(\epsilon^2 + q^2)$ , must be introduced. This ensures that we do not introduce nonphysical poles into the Green's function. Consequently, the conductivity is expressed as

$$\sigma = \frac{e^2 \nu}{h} \int_{-\infty}^0 dx' \int dq e^{iq(x-x')} q v \left( \frac{1}{\omega - v_q |q|} + \frac{1}{\omega + v_{-q} |q|} \right). \quad (\text{SV.67})$$

We can evaluate the integral over the wavevector  $q$  using the residue theorem. For this purpose, we need to find the poles of the denominator of Eq. (SV.67). To avoid having square root terms in the denominator, as  $v_q = \sqrt{(v - V_1(q))^2 - V_2(q)^2}$  we can expand the denominator

$$\sigma = \frac{e^2 \nu}{h} \int_{-\infty}^0 dx' \int dq e^{iq(x-x')} q v \left( \frac{\omega + v_q |q|}{\omega^2 - v_q^2 q^2} + \frac{\omega - v_{-q} |q|}{\omega^2 - v_{-q}^2 q^2} \right). \quad (\text{SV.68})$$

Since the denominator in Eq. (SV.68) is a polynomial in  $q$ , we can easily determine its poles. However, it is not possible to find a closed form solution for the poles analytically. Therefore, it is necessary to determine the poles numerically using a root finding algorithm. In this case, all poles are of first order. Therefore the conductivity can be expressed as in Eq. (10) in the main text.

---

[S1] X. G. Wen, Chiral Luttinger liquid and the edge excitations in the fractional quantum Hall states, *Physical Review B* **41**, 12838 (1990).

[S2] R. Fern, R. Bondesan, and S. H. Simon, Structure of edge-state inner products in the fractional quantum Hall effect, *Physical Review B* **97**, 155108 (2018).

[S3] S. H. Simon, Wavefunctionology: The Special Structure of Certain Fractional Quantum Hall Wavefunctions, in *Fractional Quantum Hall Effects* (WORLD SCIENTIFIC, 2020) pp. 377–434.

[S4] J. Dubail, N. Read, and E. H. Rezayi, Edge-state inner products and real-space entanglement spectrum of trial quantum Hall states, *Physical Review B* **86**, 245310 (2012).

[S5] X.-G. Wen, THEORY OF THE EDGE STATES IN FRACTIONAL QUANTUM HALL EFFECTS — International Journal of Modern Physics B (1992).

[S6] J. Fröhlich and U. M. Studer, Gauge invariance and current algebra in nonrelativistic many-body theory, *Reviews of modern physics* **65**, 733 (1993).

[S7] T. H. Hansson, M. Hermanns, S. H. Simon, and S. F. Viefers, Quantum Hall physics: Hierarchies and conformal field theory techniques, *Reviews of Modern Physics* **89**, 025005 (2017).

[S8] J. Fröhlich, Gauge invariance and anomalies in condensed matter physics, *Journal of Mathematical Physics* **64** (2023).

[S9] T. H. Hansson, C.-C. Chang, J. K. Jain, and S. Viefers, Conformal Field Theory of Composite Fermions, *Physical Review Letters* **98**, 076801 (2007), arxiv:cond-mat/0603125.

[S10] J. von Delft and H. Schoeller, Bosonization for beginners — repermionization for experts, *Annalen der Physik* **510**, 225 (1998).

[S11] G. Moore and N. Read, Nonabelions in the fractional quantum hall effect, *Nuclear Physics B* **360**, 362 (1991).

[S12] P. Di Francesco, P. Mathieu, and D. Sénéchal, *Conformal Field Theory*, Graduate Texts in Contemporary Physics (Springer New York, New York, NY, 1997).

[S13] D. Tong, Lectures on the Quantum Hall Effect (2016), arxiv:1606.06687 [cond-mat, physics:hep-th].

[S14] M. Padgett, J. Courtial, and L. Allen, Light's Orbital Angular Momentum, *Physics Today* **57**, 35 (2004).

[S15] K. A. Forbes and D. L. Andrews, Orbital angular momentum of twisted light: chirality and optical activity, *Journal of Physics: Photonics* **3**, 022007 (2021).

[S16] J. D. Jackson, From Lorenz to Coulomb and other explicit gauge transformations, *American Journal of Physics* **70**, 917 (2002).

[S17] C. Ciuti, Cavity-mediated electron hopping in disordered quantum Hall systems, *Physical Review B* **104**, 155307 (2021).

[S18] G. Giuliani and G. Vignale, *Quantum Theory of the Electron Liquid* (Cambridge University Press, Cambridge, 2005).